J. Micromech. Microeng. **17** (2007) 1649–1656 doi:10.1088/0960-1317/17/8/031

A low actuation voltage electrostatic actuator for RF MEMS switch applications

Chia-Hua Chu[1], Wen-Pin Shih[2], Sheng-Yuan Chung[1], Hsin-Chang Tsai[3], Tai-Kang Shing[3] and Pei-Zen Chang[1]

[1] Institute of Applied Mechanics, National Taiwan University, Taipei, Taiwan
[2] Department of Mechanical Engineering, National Taiwan University, Taipei, Taiwan
[3] Department of MEMS R&D, Delta Electronics Inc., Taoyuan, Taiwan

E-mail: wpshih@ntu.edu.tw

Received 5 May 2007, in final form 19 June 2007
Published 18 July 2007
Online at stacks.iop.org/JMM/17/1649

Abstract
This paper presents the design, fabrication and characterization of an RF MEMS switch. Low actuation voltage and high isolation of the switch were achieved by exploiting buckling and bending effects induced by well-controlled residual stress. The effects of residual stress on improving the switch performance have been investigated using both analytical and numerical methods. The proposed RF switch has been fabricated by surface micromachining. The minimum actuation voltage of the fabricated switch was measured to be 10.2 V. At a 5 GHz signal frequency, the measured insertion loss and isolation are 0.21 dB and −44 dB, respectively. These results demonstrate that low voltage and high isolation of RF MEMS switches can be achieved with proper utilization of residual stresses.

(Some figures in this article are in colour only in the electronic version)

1. Introduction

The development of highly miniaturized wireless communication systems requires full integration of circuits and radio-frequency (RF) components on a single chip. Microelectromechanical systems (MEMS) using existing semiconductor technology are promising to facilitate such integration. In a large variety of RF MEMS components, micromechanical switch has found many applications in controlling microwave signals [1–3]. Compared to its solid-state counterparts, the RF MEMS switch is superior in insertion loss, isolation and power consumption. It also has much smaller volume and weight than a conventional mechanical switch does [4]. Since the RF MEMS switch was first demonstrated by Petersen in 1979 [5], various driving mechanisms have been developed. Typical driving mechanisms of RF MEMS switches include electrostatic force, electromagnetic force, thermal expansion and piezoelectricity [5–16]. Particularly, electrostatic force is widely used because it provides the fastest switching speed and the lowest power consumption. The RF MEMS switch driven by electrostatic force also has the highest compatibility with a standard IC process. Nevertheless, in the trend of low-voltage circuitry, the large actuation voltage of electrostatic switches is still an obstacle to system integration. Reducing the actuation voltage is always at the cost of RF performance. For example, isolation for metal contact switches and insertion loss for capacitive switches could be compromised.

Typical electrostatic switches are in the form of a suspended micro-cantilever, as illustrated in figure 1(*a*). When a bias voltage is applied across the dc driving electrode pair, the contact electrode is pulled down by induced electrostatic force. For metal contact switches, signal transmission is permitted by the connection of the RF signal line with the contact electrode. The critical bias voltage to pull down the contact electrode is dominated by the air gap across the dc driving electrode pair. In the aspect of monolithic fabrication, the height of the air gap is determined by the thickness of the sacrificial layer. Although one can simply reduce the actuation voltage by using a thinner sacrificial layer, smaller gap between the contact electrode and the RF signal line will cause intolerable RF isolation of the

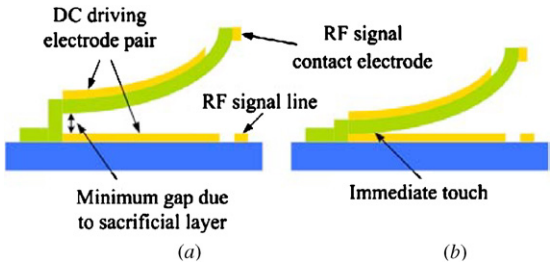

Figure 1. Schematics of cantilever beams subjected to residual stresses: (*a*) with and (*b*) without an air gap generated from the sacrificial layer.

Table 1. Simulation results of switch pull-in voltage under different sacrificial layer thicknesses.

Sacrificial layer (μm)	Stress gradient (MPa μm^{-1})	Maximum gap (μm)	Pull-in voltage (V)	Voltage reduction (%)
1.05	0	1.1	9.3	0.0
0.5	8.778	1.119	6.8	26.9
0.3	12.012	1.098	5.6	39.8
0	17.402	1.136	3.2	65.6

Note: length = 182 μm; width = 30 μm; thickness = 2 μm ; elastic constant = 275 GPa; dielectric layer = 0.05 μm.

switch. To prevent this compromise, residual stresses have been used to bend up the micro-cantilever to achieve large separation between the RF signal line and contact electrode [17–19]. Nevertheless, the reduction of actuation voltage is still limited by the inevitable sacrificial layer. Ideally, the actuation voltage can be substantially reduced if one could fabricate a switch without using sacrificial layers, as illustrated in figure 1(*b*). Under this circumstance, gradient stress is required to bend up the micro-cantilever for RF isolation. For a given micro-cantilever switch, we have used a finite element method to calculate its driving voltage under different gap heights. The simulation results are summarized in table 1. For this particular switch, the simulation result shows that a 65.6% reduction of actuation voltage can be achieved in the absence of the sacrificial layer. Gradient stress of 17.402 MPa μm^{-1} is applied to obtain the 1.136 μm gap height between the RF signal line and the contact electrode in this case. In reality, it is impossible to make suspended micro-cantilever without using sacrificial layers in practical monolithic fabrication. To effectively reduce the actuation voltage, a proper mechanical design is necessary to reduce the air gap inherited from the sacrificial layer.

This paper presents the design, fabrication and characterization of an RF MEMS switch which simultaneously possesses low actuation voltage and high isolation. These particular switch characteristics are achieved by exploiting buckling and bending effects resulting from well-controlled residual stresses. The switch consists of a fixed–fixed beam and two cantilever beams, as depicted in figure 2. The fixed–fixed beam buckles due to sufficient uniform stress, and the buckling direction is governed by gradient stresses. Therefore, the gap between the dc driving electrode pair is dramatically reduced, resulting in significant decrease of actuation voltage. Similarly, large tip deflection

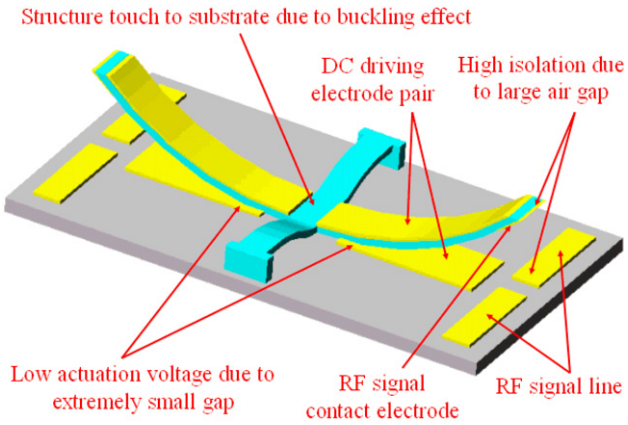

Figure 2. Schematics of the proposed RF MEMS switch.

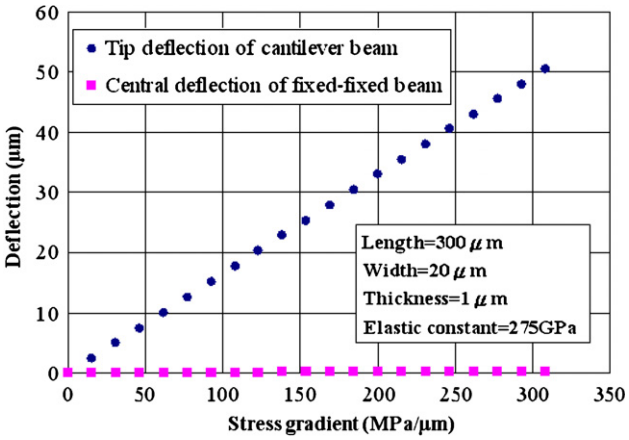

Figure 3. Simulated deflections of the cantilever beam and fixed–fixed beam under given gradient stresses.

of the cantilever beams is achieved by utilizing gradient stress so that the switch isolation is improved.

2. Residual stress

Residual stresses induced by fabrication process or thermal mismatch can be divided into gradient stress and uniform stress. Gradient stress causes bending moments which result in transverse deflection of micro-beams. The direction of beam deflection can be easily controlled by using different gradient profiles of the residual stresses and proper mechanical constraints. To illustrate this concept, finite element analysis using ANSYS software was conducted to simulate deflections of a fixed–fixed beam and a cantilever beam, respectively. In the analysis, stress induced by thermal loads was employed to simulate gradient stresses. Specifically, thermal loads were applied so that the upper and lower surfaces of the beams are subjected to compressive and tensile stresses, respectively. The simulation result in figure 3 indicates that gradient stress causes large deflection in the cantilever beam but negligible deflection in the fixed–fixed beam. The small deflection of the fixed–fixed beam is due to stringent boundary constraints. As anticipated, the cantilever beam bends upward under this particular gradient profile.

The simulation result indicates that the stress gradient also induces non-negligible bending moment along the direction of

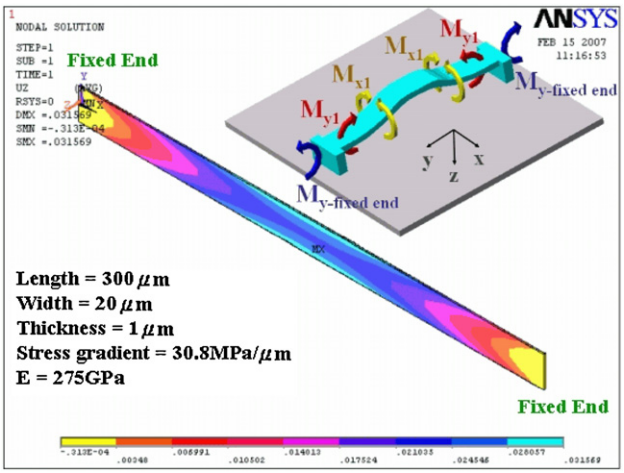

Figure 4. Simulated deflection of a fixed–fixed beam under gradient stress.

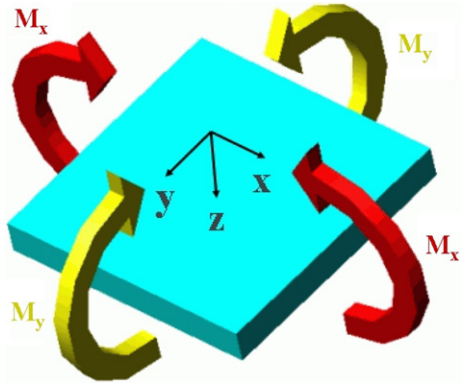

Figure 5. Sign convention for positive moments.

beam span (M_{x1} in the inset of figure 4). This bending moment plays a significant role in controlling the buckling direction of the fixed–fixed beam. This is because the central part of the fixed–fixed beam exhibits plate characteristics when bending moments from two orthogonal directions are considered. The moments and curvatures of a plate are given by [20]

$$M_x = D\left(\frac{1}{r_x} + \nu\frac{1}{r_y}\right) = -D\left(\frac{\partial^2 w}{\partial x^2} + \nu\frac{\partial^2 w}{\partial y^2}\right)$$
$$M_y = D\left(\frac{1}{r_y} + \nu\frac{1}{r_x}\right) = -D\left(\frac{\partial^2 w}{\partial y^2} + \nu\frac{\partial^2 w}{\partial x^2}\right) \qquad (1)$$
$$D = \frac{Eh^3}{12\left(1-\nu^2\right)}$$

where M_x, $M_y \equiv$ moments per unit length acting on the plate edges parallel to y and x axes, respectively, $\frac{1}{r_x}, \frac{1}{r_y} \equiv$ curvatures of surfaces parallel to xz and yz planes, respectively, $w \equiv$ deflection in the z-direction, $h \equiv$ plate thickness, $E \equiv$ modulus of elasticity, $\nu \equiv$ Poisson's ratio.

Moments are considered positive if they produce compression in the upper part of the plate and tension in the lower part, as shown in figure 5. Curvature is also considered positive if it is convex toward the positive z-direction. Note that the fixed–fixed beam is constrained along the y-axis as illustrated in figure 4. Therefore, the bending moments M_{y_1} induced by gradient stress is compensated by the fixed-end reaction $M_{y\text{-fixed end}}$, resulting in zero resultant moments M_y. Substituting $M_y = 0$ and non-zero M_x into equation (1) gives a positive curvature $1/r_x$ and a small negative curvature $1/r_y$. The fact that Poisson's ratio is smaller than unity has been applied in using equation (1). The positive curvature $1/r_x$ indicates that the plate is convex toward the positive z-direction. On the other hand, the negative curvature $1/r_y$ indicates the plate is convex toward the negative z-direction from an orthogonal viewpoint. A saddle-shaped plate is consequently formed in the central part of the fixed–fixed beam, resulting in a small upward deflection. The simulation result shown in figure 4 agrees with the reasoning given above.

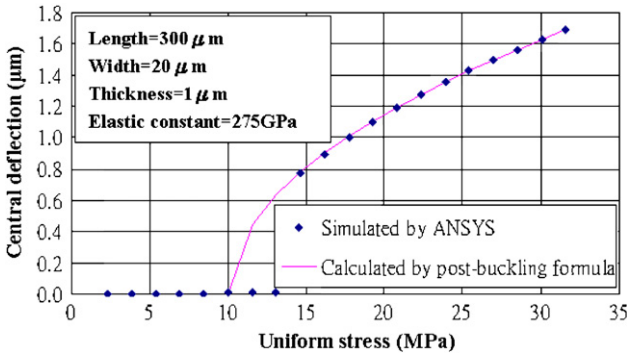

Figure 6. Comparison of simulation and analytical results of central deflection of a fixed–fixed beam which is subjected to uniform compressive stress.

Since gradient stress has been found insufficient to generate large deflection of the fixed–fixed beam, uniform compressive stress must be applied for buckling phenomenon to occur. Our simulation result in figure 6 shows that uniform stress causes a relatively large transverse deflection compared to that due to gradient stress. From classical Euler buckling analysis, the critical stress σ_{cr} to buckle a fixed–fixed beam is [21]

$$\sigma_{cr} = \frac{\pi^2 E h^2}{3L^2} \qquad (2)$$

where L is the beam length. Substituting $E = 275$ GPa, $L = 300$ μm and $h = 1$ μm into equation (2) gives $\sigma_{cr} = 10.1$ MPa. Finite element analysis was also used to evaluate the critical stress and gives a relatively larger result, namely $\sigma_{cr} = 13$ MPa. Nevertheless, the simulated central deflection of the fixed–fixed beam (ω_{max}) in post-buckling regime agrees well with the post-buckling formula [22]:

$$\omega_{max} = \pm\sqrt{\frac{4\varepsilon L^2}{\pi^2} - \frac{16I}{A}} \qquad (3)$$

where ε is the strain induced by uniform residual stress, I and A stand for moment of inertia and cross-sectional area of the beam, respectively. Figure 6 shows the comparison between the simulation results and equation (3). Both the numerical and analytical results indicate predictable deflection when the fixed–fixed beam is subjected to uniform compressive stress. By applying both gradient stress and uniform compressive stress on the fixed–fixed beam, the direction as well as the magnitude of the beam deflection can be controlled, as shown in figure 7.

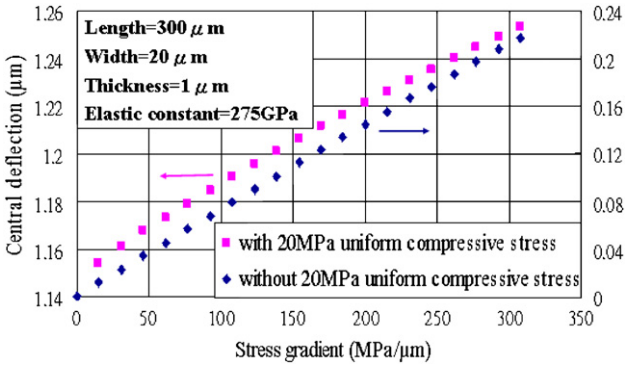

Figure 7. Simulated central deflection of the fixed–fixed beam which is subjected to gradient stress. Additional effects of uniform compressive stress on the deflection are evaluated.

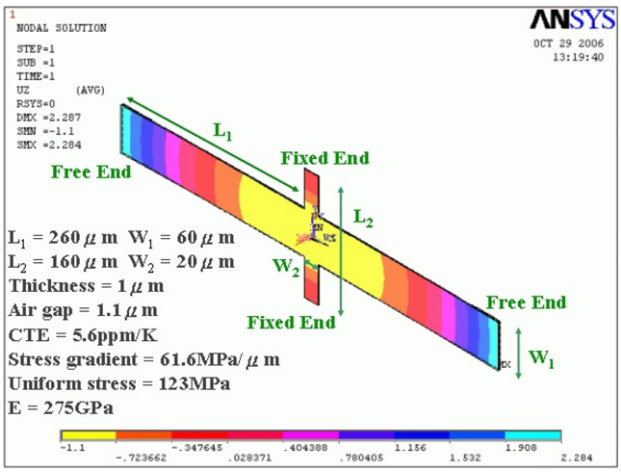

Figure 8. Simulated deflection of the proposed switch subjected to stress gradient and uniform compressive stress.

3. Structure design

In order to reduce actuation voltage and increase RF isolation simultaneously, a crisscross-shaped electrostatic switch is proposed. This single-pole-double-throw switch consists of a fixed–fixed beam and two cantilever beams, as depicted in figure 2. The RF contact electrodes are positioned at the free end of the cantilever beams, respectively. Note that the whole structure is subjected to identical gradient stress and uniform compressive stress. The gradient stress is designed to produce positive bending moment so that the cantilever beams deflect upwards. As a result, high RF isolation can be achieved by increasing the air gap between RF signal electrodes. To reduce the actuation voltage of the switch by reducing the air gap between the dc driving electrode pair, uniform compressive stress should be applied. This uniform compressive stress is intended to buckle the fixed–fixed beam downward. Figure 8 shows the anticipated design and simulation result. Under proper gradient stress and uniform compressive stress, the central part of the switch buckles and touches the substrate. Meanwhile, the free ends of the cantilever beams bend upward so that sufficient air gap for RF isolation is generated.

It should be noted that the buckling direction of the electrostatic switch can be controlled by using proper geometry

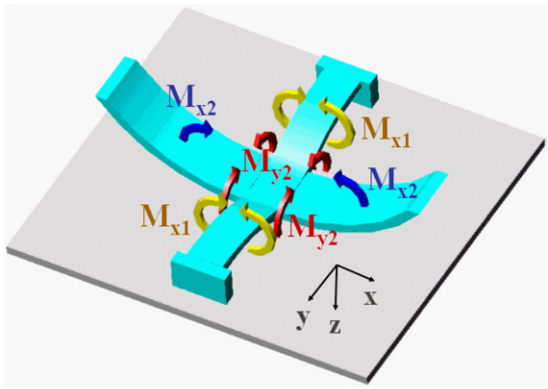

(*a*)

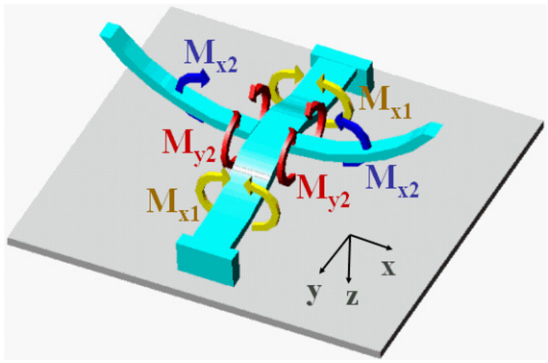

(*b*)

Figure 9. Moment distribution induced by gradient stress in a proposed switch structure: (a) with wide cantilever beams; (b) with narrow cantilever beams.

design. Particularly, the width of the cantilever beams plays a significant role in controlling the buckling direction. If the width of the cantilever beams (W_1) is sufficiently large, plate behavior at the central part of the fixed–fixed beam becomes prominent. Under this circumstance, the gradient stress in the cantilever beams induces bending moments (M_{y2}) at the central part of the fixed–fixed beam, as illustrated in figure 9(*a*). Since the whole switch is subjected to identical gradient stress, M_{y2} is equal to M_{x1}. According to equation (1), positive M_x and M_y lead to the positive curvatures $1/r_x$ and $1/r_y$. As a result, the central part of the fixed–fixed beam deflects downward to the positive z-direction. Contradictorily, if the cantilever beams have relatively small width, their bending moments exerting on the central part of the fixed–fixed beam become negligible. Under this circumstance, M_{y2} becomes negligible, causing the fixed–fixed beam to buckle upward as illustrated in figure 9(*b*).

Finite element analysis has been carried out to determine the critical width of the cantilever beams at which the fixed–fixed beam changes buckling direction. Let W_1 and W_2 be the widths of the cantilever beams and the fixed–fixed beam, respectively. The simulation result in figure 10 indicates that the switch buckles upward when $W_1/W_2 < 1.15$ and downward when $W_1/W_2 > 1.35$.

To minimize the actuation voltage of our electrostatic switch, the deflection at the central part of the fixed–fixed beam should be greater than the thickness of the sacrificial layer underneath. For typical MEMS fabrication, the thickness of the sacrificial layer is 1–2 μm. When the switch footprint

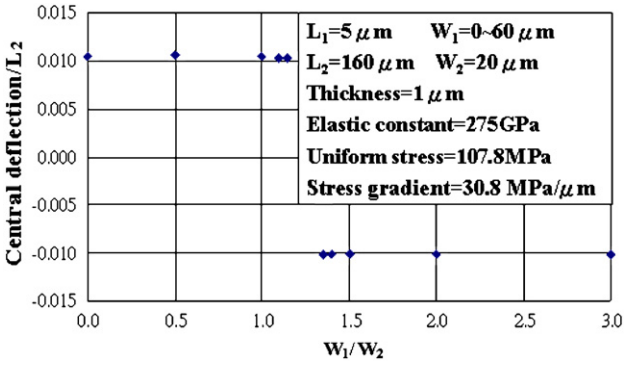

Figure 10. Simulated central deflection of the switch as a function of the W_1/W_2 ratio.

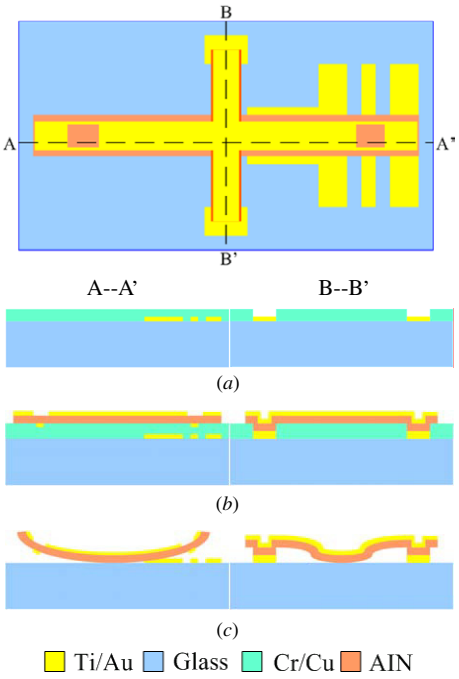

Figure 11. Fabrication process of the RF MEMS switch. (*a*) Deposition and patterning of the lower electrode and the sacrificial layer. (*b*) Deposition and patterning of the contact metal, AlN and the upper electrode, respectively. (*c*) Releasing the switch.

is constrained, the deflection of the fixed–fixed beam can be increased by increasing the uniform compressive stress. Conversely, when a fixed uniform compressive stress is given, large deflection can be achieved by adopting a longer and thinner fixed–fixed beam. To obtain high RF isolation, large tip displacement of the cantilever beams in our electrostatic switch is required. This can be achieved by increasing gradient stress or adopting longer and thinner cantilever beams.

4. Fabrication and measurement results

The electrostatic switch is fabricated by applying surface micromachining on the glass substrate, as illustrated in figure 11. The lower electrode and co-planer waveguide (CPW) are made of Ti/Au (20 nm/200 nm) layers. The width of the CPW signal line is 20 μm. The gap between the signal line and the ground lines is 2 μm. These metal layers

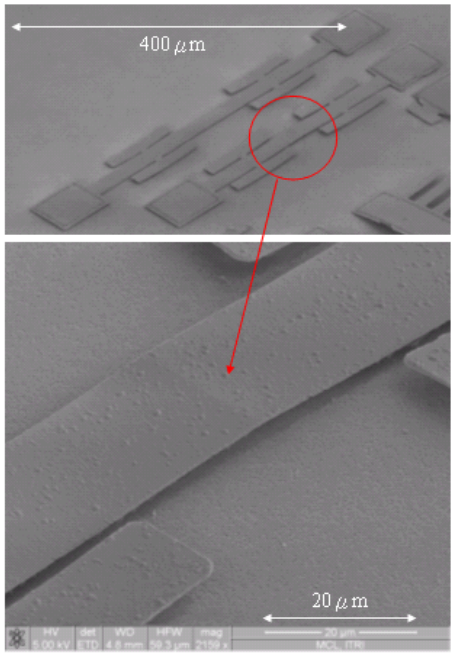

Figure 12. SEM images of the fixed–fixed beam which buckles upward.

are first deposited and patterned by e-beam evaporation and wet etching, respectively. In demonstrating the switch workability, the metal thickness of 0.2 μm is used so that the fabrication can be simplified. To achieve high power or low loss of the signal transmission, the metal thickness of the CPW should be increased. The Cu sacrificial layer between the signal line and the contact electrode is then deposited and patterned by e-beam evaporation and lift-off process, respectively (figure 11(*a*)). The thickness of the sacrificial layer is 1 μm. On the sacrificial layer, the Au/Ti (200 nm/20 nm) contact metal is deposited and patterned by e-beam evaporation and wet etching, respectively. Then the main mechanical structure layer, which is made of AlN, is deposited by the sputtering process. On the AlN layer, the Ti/Au (20 nm/200 nm) upper electrode is deposited and defined by the lift-off process (figure 11(*b*)). Finally, the whole structure is released in the chromium etchant Cr-7 (figure 11(*c*)).

The control of residual stress in the AlN film is the major challenge in the fabrication. It affects the curvature of the cantilever beam, central displacement of the fixed–fixed beam and the pull-in voltage. It has been shown that the residual stress in sputtered AlN films can be controlled by changing the sputtering power, deposition rate, ratios of Ar and N_2 gases, distance between the target to the substrate and magnetic field intensity [23, 24]. Using fixed deposition parameters, repeatable residual stresses have been obtained in this work.

In the test structures of the fixed–fixed beam, a buckling phenomenon due to the uniform compressive stress has been observed. Without attaching cantilever beams on the fixed–fixed beam, the central part of the fixed–fixed beam buckles upward, as shown in figure 12. If the fixed–fixed beam is connected to two cantilever beams as shown in figure 13, its central part buckles downward to the substrate. Meanwhile, the free ends of the cantilever beams bend upward

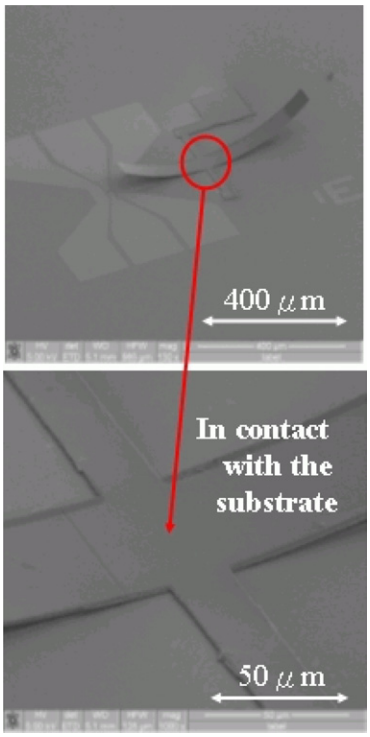

Figure 13. SEM images of the fabricated switch which buckles downward.

as anticipated. In this case, the air gap between a dc electrode pair gradually decreases from the free end to the anchor of the cantilever beams. As a result, the actuation voltage of the switch is reduced. Nevertheless, it should be noted that the actuation voltage could be increased if over large curvature of the cantilever beams is induced by the gradient stress.

The fabricated switch is shown in figure 14, and its dimensions are given in figure 8. A bias voltage is applied across the upper electrode and the CPW ground to actuate the switch. As the applied voltage incrementally increases to the pull-in voltage of the switch, the curved cantilever beam gradually bends down from the region of small gap to the region of large gap.

The pull-in voltage of the switch is measured to fall between 10.2 and 70 V due to large gradient stress which is in the same level of the simulation results given in figure 15. With the 20 μm free-end height of the switch, the measured pull-in voltage and releasing voltage are 15.3 V and 7.9 V, respectively. The measured pull-in voltage deviates from the simulation result by 50%. This discrepancy is mainly from different material properties such as Young's modulus, Poisson's ratio and dielectric constant between the deposited AlN film and the parameters used in the simulation. Nevertheless, the measured results show the same trend of the pull-in voltage as a function of the initial tip height as the simulation results do. These results indicate that the proposed switch has much lower pull-in voltage compared to that of the typical cantilever switch. The simulation results also show that increasing the initial tip height of the switch, i.e. increasing the curvature of the bending beam, will increase the actuation voltage. Nevertheless, the increased actuation voltage is still smaller than that of conventional cantilever switches in which residual stresses are not utilized. This comparison indicates

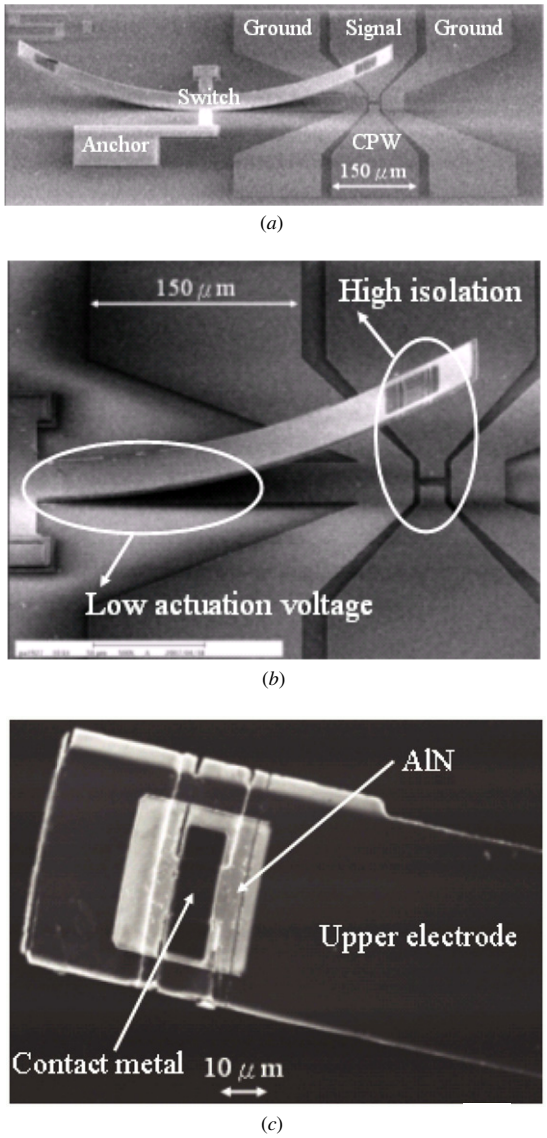

Figure 14. SEM images of the fabricated switch. Whole structure (*a*) and (*b*) and contact metal (*c*).

that the presented switch can efficiently reduce the actuation voltage without sacrificing RF isolation.

The free-end height of the fabricated switch was measured to be 20 μm. Finite element simulation indicates that such free-end height is induced by the gradient stress of 125 MPa μm^{-1}. When the pull-in voltage of 15.3 V is applied, the finite element simulation indicates that the corresponding contact force is 73.2 μN. This value is sufficient to provide stable contact resistance for soft metal materials such as gold [25]. Lowering the gradient stress of the switch will increase the contact force.

The performance of the fabricated switch at high frequency was measured by a network analyzer (Agilent 8722ES). The measured insertion loss and isolation at 5 GHz are 0.21 dB and –44 dB, respectively, as shown in figure 16. These results demonstrate that the presented device concept can reduce the actuation voltage and improve isolation of RF MEMS switches. Low insertion loss can also be achieved.

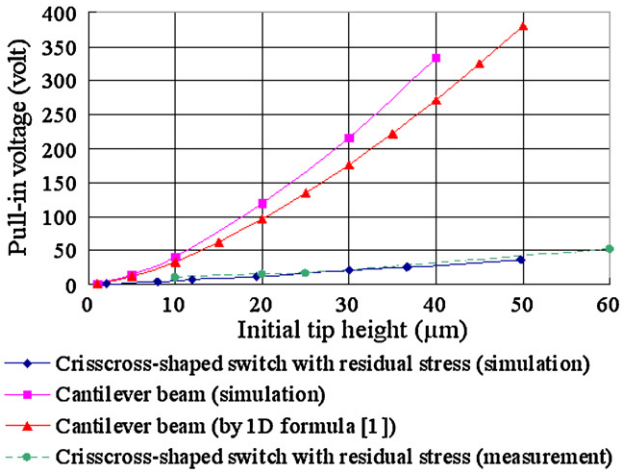

Figure 15. Simulated pull-in voltage as a function of the initial tip height of the fabricated switch.

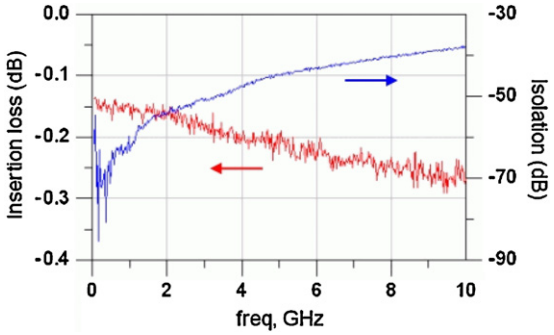

Figure 16. Characterized insertion loss and isolation of the fabricated switch.

5. Summary

A low voltage and high isolation RF MEMS switch has been successfully demonstrated by utilizing residual stress which induces desirable buckling and bending effects. The buckling effect induced by uniform compressive stress eliminates the air gap inherited from the sacrificial layer so that the actuation voltage of the switch is reduced. Gradient stress causes bending moment which increases tip height of the cantilever beam in the switch, resulting in enhanced RF isolation. The buckling direction of the fabricated switch was found to be dominated by the width ratio of the cantilever beams to the fixed–fixed beam. The minimum actuation voltage of the fabricated switch was measured to be 10.2 V. At 5 GHz, the measured insertion loss and isolation are 0.21 dB and –44 dB respectively. These results demonstrate that low voltage and high isolation RF MEMS switches can be achieved with proper utilization of residual stresses.

Acknowledgments

The authors would like to thank Delta Electronics for technical support and service. The device was fabricated at the NTU Nano-Electro-Mechanical-Systems Research Center. This project was funded by the National Science Council, Taiwan, project no NSC 95-2221-E-002-241.

References

[1] Rebeiz G M and Muldavin J B 2001 RF MEMS switches and switch circuits *IEEE Microw. Mag.* **2** 59–71
[2] Yao J J 2000 RF MEMS from a device perspective *J. Micromech. Microeng.* **10** R9–R38
[3] de Los Santos H J, Fischer G, Tilmans H A C and van Beek J T M 2004 RF MEMS for ubiquitous wireless connectivity: part 1. Fabrication *IEEE Microw. Mag.* **5** 36–49
[4] Grant P D, Denhoff M W and Mansour R R 2004 A comparison between RF MEMS switches and semiconductor switches *Proc. Int. Conf. MEMS, NANO and Smart Systems (ICMENS'04) (Banff, Alberta, Canada)* pp 515–21
[5] Petersen K E 1979 Micromechanical membrane switch on silicon *IBM J. Res. Dev.* **23** 376–85
[6] Goldsmith C, Lin T H, Powers B, Wu W R and Norvell B 1995 Micromechanical membrane switches for microwave applications *Proc. IEEE MTT-S Int. Microwave Symp. Digest (Orlando, FL)* vol 1 pp 91–4
[7] Hah D Y, Yoon E S and Hong S C 2000 A low voltage actuated micromachined microwave switch using torsion springs and leverage *IEEE Trans. Microw. Theory* **48** 2540–5
[8] Peroulis D, Pacheco S P, Sarabandi K and Katehi L P B 2003 Electromechanical considerations in developing low-voltage RF MEMS switches *IEEE Trans. Microw. Theory* **51** 259–70
[9] Chan R, Lesnick R, Becher D and Feng M 2003 Low-actuation voltage RF MEMS shunt switch with cold switching lifetime of seven billion cycles *J. Microelectromech. Syst.* **12** 713–9
[10] Nishijima N, Hung J J and Rebeiz G M 2004 A low-voltage high contact force RF-MEMS switch *Proc. IEEE MTT-S Int. Microwave Symp. Digest (Fort Worth, TX)* vol 2 pp 577–80
[11] Nakatani T, Nguyen A T, Shimanouchi T, Imai M, Ueda S, Sawaki I and Satoh Y 2005 Single crystal silicon cantilever-based RF-MEMS switches using surface processing on SOI *Proc. 18th IEEE Int. Conf. on Micro Electro Mechanical Systems (Miami Beach, FL)* pp 187–90
[12] Robert P, Saias D, Billard C, Boret S, Sillon N, Maeder-Pachurka C, Charvet P L, Bouche G, Ancey P and Berruyer P 2003 Integrated RF-MEMS switch based on a combination of thermal and electrostatic actuation *Proc. 12th Int. Conf. Solid Stale Sensors, Actuators and Microsystems (Transducers 2003) (Boston, MA)* vol 2 pp 1714–7
[13] Moseley R W, Yeatman E M, Holmes A S, Syms R R A, Finlay A P and Boniface P 2006 Laterally actuated, low voltage, 3-port RF MEMS switch *Proc. 19th IEEE Int. Conf. on Micro Electro Mechanical Systems (Istanbul, Turkey)* pp 878–81
[14] Borwick III R L, Stupar P A and DeNatale J 2003 A hybrid approach to low-voltage MEMS switches *Proc. 12th Int. Conf. on Solid Stale Sensors, Actuators and Microsystems (Transducers 2003) (Boston, MA)* vol 1 pp 859–62
[15] Cho I J, Song T, Baek S H and Yoon E 2005 A shunt-type RF MEMS switch at 3.3 V operation actuated by Lorentz force and electrostatic hold *Proc. 13th Int. Conf. on Solid Stale Sensors, Actuators and Microsystems (Transducers 2005) (Seoul, Korea)* vol 1 pp 1051–4
[16] Lee H C, Park J Y and Bu J U 2005 Piezoelectrically actuated RF MEMS DC contact switches with low voltage operation *IEEE Microw. Wireless Compon. Lett.* **15** 202–4
[17] Duffy S, Bozler C, Rabe S, Knecht J, Travis L, Wyatt P, Keast C and Gouker M 2001 MEMS microswitches for reconfigurable microwave circuitry *IEEE Microw. Wireless Compon. Lett.* **11** 106–8
[18] Muldavin J, Bozler C and Keast C 2006 Wafer-scale packaged RF-MEMS switches *Proc. IEEE MTT-S Int. Microwave Symp. Digest (San Francisco, CA)* pp 267–70

[19] Chang C L and Chang P Z 2000 Innovative micromachined microwave switch with very low insertion loss *Sensors Actuators* A **79** 71–5
[20] Timoshenko S P and Woinowsky-krieger S 1959 *Theory of Plates and Shells* 2nd edn (New York: McGraw-Hill) pp 33–9
[21] Gere J M and Timoshenko S P 1997 *Mechanics of Materials* 4th edn (Boston, MA: PWS Publishing Company) pp 751–2
[22] Fang W and Wickert J A 1994 Post-buckling of micromachined beams *J. Micromech. Microeng* **4** 182–7
[23] Dubois M A and Muralt P 2001 Stress and piezoelectric properties of aluminum nitride thin films deposited onto metal electrodes by pulsed direct current reactive sputtering *J. Appl. Phys.* **89** 6389–95
[24] Lee S H, Yoon K H, Cheong D S and Lee J K 2003 Relationship between residual stress and structural properties of AlN films deposited by r.f. reactive sputtering *Thin Solid Films* **435** 193–8
[25] Oberhammer J and Stemme G 2006 Active opening force and passive contact force electrostatic switches for soft metal contact materials *IEEE J. Microelectromech. Syst.* **15** 1235–42